Differential Approximation, Scaling to 10K Cores, and NIMROD/ELITE Comparison

Carl Sovinec and Bonita Burke
University of Wisconsin-Madison

CEMM Meeting
November 1, 2009
Atlanta, Georgia

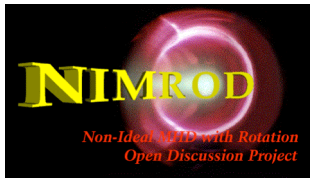

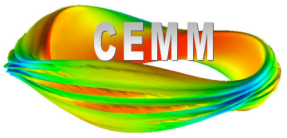

Outline: 3 Topics

- Differential approximation
  - Key findings von Neumann analysis (review)
  - Applying DA to implicit leapfrog
  - Insights from DA
- Benchmarking of NIMROD with ELITE
  - Quick review of study
  - ‘Final’ ballooning-unstable comparisons
- Parallel scaling
  - Algorithm improvements (from last year)
  - Recent results
- Conclusions

Differential Approximation→Background

Analyzing modes of the time-step operation (von Neumann) was critical in the development of NIMROD's implicit leapfrog algorithm for two-fluid models (SciDAC '05).

- The analysis includes Hall, gyroviscosity, electron inertia, separate COM and electron flows, and resistivity.
- Thermal response is adiabatic with electron pressure being a fixed fraction of the total pressure.
- Spatially, the linear response is assumed to vary as exp(*iky*).
  - Spatial discretization effects are not considered.
- λ is the eigenvalue of the time-step operation.
  - Modes satisfy:

$$\begin{pmatrix} \underline{v}^{j+1} \\ \underline{b}^{j+3/2} \\ p^{j+3/2} \end{pmatrix} = \lambda \begin{pmatrix} \underline{v}^{j} \\ \underline{b}^{j+1/2} \\ p^{j+1/2} \end{pmatrix}$$

Results of the von Neumann analysis establish the stability of the implicit leapfrog.

- The time-step matrix is found from products of matrices for explicit terms and inverses of matrices for implicit terms.
- Analytical relations for the eigenvalues can be found for limiting cases.
- Results for general cases are evaluated numerically with LAPACK routines that can handle matrices with geometric multiplicity < algebraic multiplicity.
- Key findings (presented at APS 2005 & Sherwood 2006) are:
  - **The implicit leapfrog is numerically stable with the Hall and GV terms centered in the B- and V- advances, respectively.**
  - **Predictor/corrector advection leads to severe time-step restrictions with the implicit Hall advance.**
  - **Implicit advection is numerically stable if $\mathbf{V}\cdot\nabla$ terms are centered in each advance.**
  - **Dissipation is numerically stable for centered or backward differencing.**

Numerical evaluation produces eigenvectors that can be used to initialize NIMROD tests.

- The equations are normalized such that time is in units of $1/\Omega_i$ and length is in units of d_i.
- Eigenvectors reflect the algorithm's temporal staggering, which is critical for launching a single sine-wave at finite Δt-values.

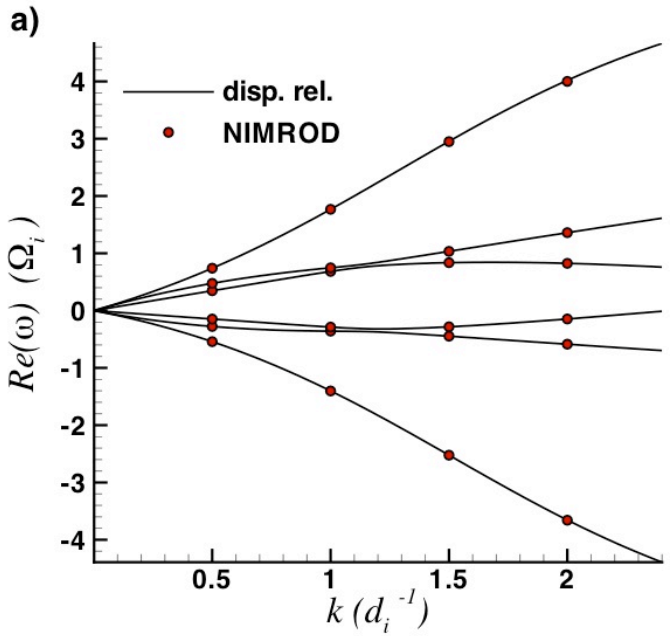

Case with nearly parallel propagation has β=0.15, V_0=0.2, and Δt=0.5.

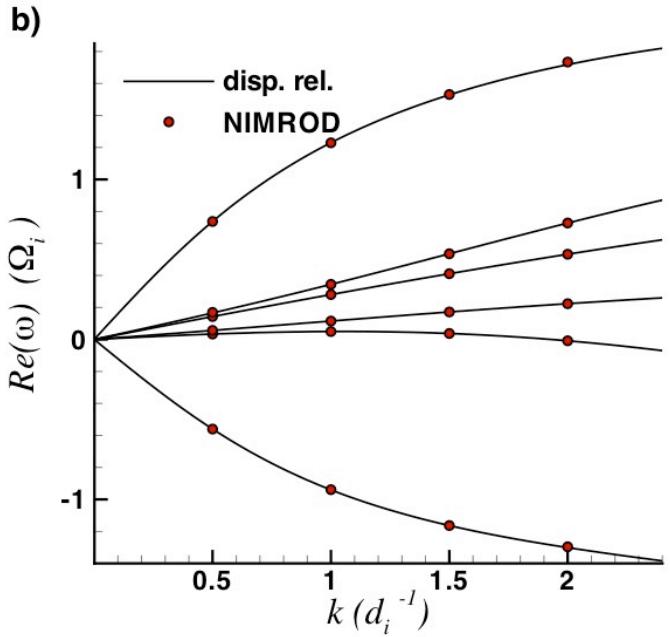

Case with nearly perp. propagation has β=0.6, V_0=0.2, and Δt=1.5.

- The agreement (including GV effects) contributes to code verification.

Numerical evaluation is also used to compare accuracy with the Crank-Nicolson method.

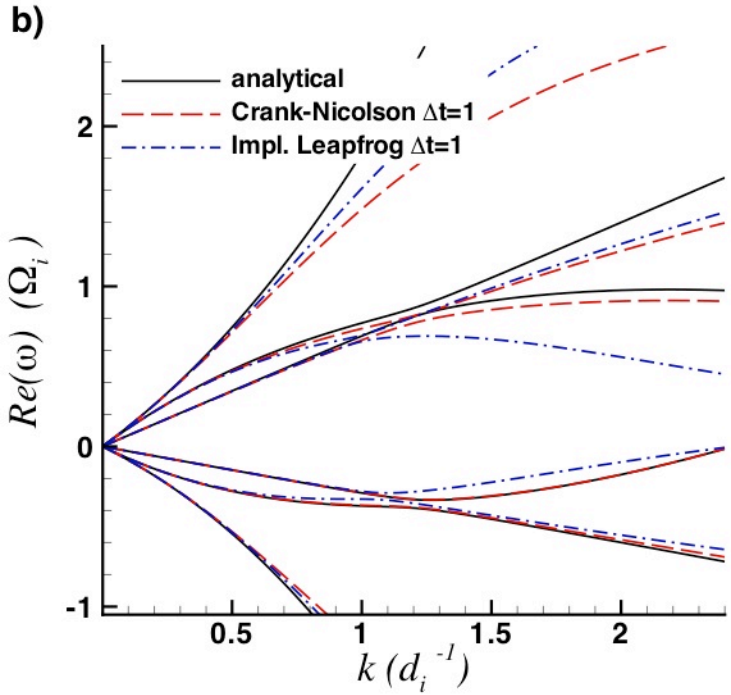

Comparison for nearly parallel propagation has β=0.15, V_0=0.2, and Δt=1.

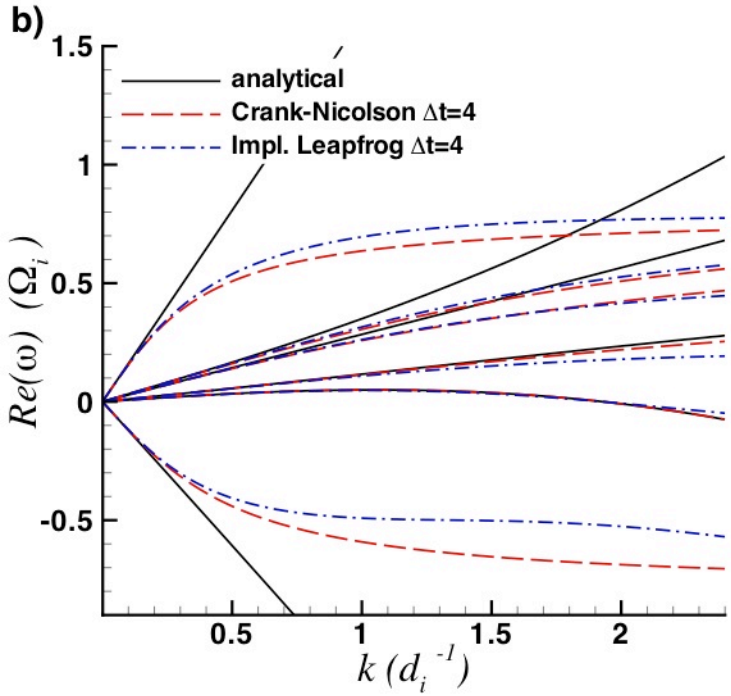

Comparison with nearly perp. propagation has β=0.6, V_0=0.2, and Δt=4.

- As reported previously, the accuracy of the implicit leapfrog is comparable to that of Crank-Nicolson for most plane-wave responses.
- The semi-implicit operator in the implicit leapfrog suppresses effects of the ion cyclotron resonance for the low-frequency parallel mode when $k\Delta t \sim 1$.
  - This error from splitting (Knoll, JCP **185**, '03) seems tolerable.

Differential approximation (Shokin, Springer-Verlag '83) helps explain the cause of numerical instabilities with poor selection of parameters.

- It also provides insight and increases confidence that the von Neumann findings are representative.
- We have used it to consider
  - The centering of resistive dissipation
  - Compatibility of implicit advection with the staggered leapfrog
  - The influence of the semi-implicit operator with centered advection
  - Compatibility of the semi-implicit velocity advance with implicit Hall in the magnetic-field advance.
- In general, differential approximation provides only necessary conditions for numerical stability.

Our approach follows Caramana (JCP 96, '91), but we address the temporal staggering directly.

- Time is normalized by $1/\Omega_i$; length is normalized by d_i; $v_A \rightarrow 1$.
- For perpendicular propagation at low-k and $\beta \rightarrow 0$, the algorithm is

$$\left(1-\Delta t^2 C_0 \frac{\partial^2}{\partial y^2}\right)\frac{v^{j+1}-v^j}{\Delta t} = -V_0 \frac{\partial}{\partial y}\left[\theta_v v^{j+1} + (1-\theta_v)v^j\right] - \frac{\partial}{\partial y} b^{j+1/2}$$

$$\frac{b^{j+3/2}-b^{j+1/2}}{\Delta t} = -V_0 \frac{\partial}{\partial y}\left[\theta_b b^{j+3/2} + (1-\theta_b)b^{j+1/2}\right] - \frac{\partial}{\partial y} v^{j+1} \quad ,$$

where v is the y-component, and b is parallel to $\mathbf{B}_0$.

- We expand v about half-integer levels and b about integer levels and drop terms that would require additional initial conditions (Caramana).

$$\left(1-\Delta t^2 C_0 \frac{\partial^2}{\partial y^2}\right)\left.\frac{\partial v}{\partial t}\right|_{t_{1/2}} = -V_0 \frac{\partial}{\partial y}\left[v + \Delta t\left(\theta_v - \frac{1}{2}\right)\frac{\partial v}{\partial t}\right]_{t_{1/2}} - \frac{\partial}{\partial y}\left(b - \frac{\Delta t}{2}\frac{\partial b}{\partial t}\right)_{t_1}$$

$$\left.\frac{\partial b}{\partial t}\right|_{t_1} = -V_0 \frac{\partial}{\partial y}\left[b + \Delta t\left(\theta_b - \frac{1}{2}\right)\frac{\partial b}{\partial t}\right]_{t_1} - \frac{\partial}{\partial y}\left(v + \frac{\Delta t}{2}\frac{\partial v}{\partial t}\right)_{t_{1/2}} \quad ,$$

- Last terms on the right include terms that account for synchronization.

Manipulation of the differential approximation shows the need for centered advection.

- Change to sum and difference variables, and substitute

$$v = (Z_+ + Z_-)/2 \qquad b = (Z_+ - Z_-)/2$$

- To order Δt^1, the system can be written as

$$\frac{\partial}{\partial t} Z_\pm = -V_0 \frac{\partial}{\partial y} Z_\pm \mp \frac{\partial}{\partial y} Z_\pm$$
$$+ \frac{\Delta t}{2}\left(V_0^2 \pm V_0\right)\left(\theta_v + \theta_b - 1\right)\frac{\partial^2}{\partial y^2} Z_\pm - \frac{\Delta t}{2}\left[V_0^2\left(\theta_b - \theta_v\right) \mp V_0\left(\theta_b - \theta_v + 1\right) + 1\right]\frac{\partial^2}{\partial y^2} Z_\mp \ .$$

- Analytically (order Δt^0), the two waves propagate independently and in opposite directions in a frame moving with the flow.
- Considering the 3rd term on the rhs, for V_0<1, one of the two numerical responses dissipates and the other is ill-posed when $\theta_v + \theta_b \neq 1$.
  - This explains why backward (& forward) differencing is not stable.
  - Stability with backward differencing for V_0>1 has been confirmed with von Neumann computations.
- More truncation errors are eliminated with θ_v=θ_b. Other contributions to the last term are from synchronization (not $O(\Delta t)$ errors).

Differential approximation also shows the compatibility of centered advection and the semi-implicit advance.

- The equations can be manipulated into a second-order wave equation.

$$\left[1-\Delta t^2\left(C_0-\frac{1}{4}\right)\frac{\partial^2}{\partial y^2}\right]\frac{\partial^2 v}{\partial t^2}+V_0\left(2-\Delta t^2 C_0\frac{\partial^2}{\partial y^2}\right)\frac{\partial}{\partial y}\frac{\partial v}{\partial t}+\left(V_0^2-1\right)\frac{\partial^2}{\partial y^2}v=0$$

- For $C_0 \geq 1/4$, the operator acting on the highest temporal derivative is a positive differential operator in the sense that

$$\int A\left[1-\Delta t^2\left(C_0-\frac{1}{4}\right)\frac{\partial^2}{\partial y^2}\right]A\,dy=\int\left[A^2+\Delta t\left(C_0-\frac{1}{4}\right)\left(\frac{\partial A}{\partial y}\right)^2\right]dy\geq 0$$

  with homogeneous boundary conditions.

- This is related to the effective *k*-dependent inertia described by Schnack (JCP **70**, '87) and by Caramana.

- For infinite or periodic systems, where Fourier rep. is appropriate, solutions of the characteristic equation are real for $C_0 \geq 1/4$ for all Δt-values.

$$\omega_k=\frac{kV_0\left(1+\frac{C_0}{2}k^2\Delta t^2\right)\pm k\sqrt{1+k^2\Delta t^2\left(C_0+\frac{V_0^2}{4}-\frac{1}{4}\right)+\frac{C_0^2}{4}V_0^2k^4\Delta t^4}}{1+\left(C_0-\frac{1}{4}\right)k^2\Delta t^2}$$

Compatibility of centered Hall and the semi-implicit advance follows from similar reasoning.

- Here, we consider parallel propagation at arbitrary k with V_0=0 and $\beta \to 0$.

$$\left(\frac{1}{\Delta t} - \Delta t C_0 \frac{\partial^2}{\partial y^2}\right)\left(\underline{v}^{j+1} - \underline{v}^{j}\right) = \frac{\partial}{\partial y}\underline{b}^{j+1/2}$$

$$\frac{1}{\Delta t}\left(1 - \frac{m_e}{m_i}\frac{\partial^2}{\partial y^2}\right)\left(\underline{b}^{j+3/2} - \underline{b}^{j+1/2}\right) = \frac{\partial}{\partial y}\underline{v}^{j+1} + \frac{1}{2}\begin{pmatrix} 0 & -1 \\ 1 & 0 \end{pmatrix}\frac{\partial^2}{\partial y^2}\left(\underline{b}^{j+3/2} + \underline{b}^{j+1/2}\right)$$

- The $\underline{v}$ and $\underline{b}$ vectors have x- and z-components.
- After expanding we arrive at

$$\left[\left(1 - \Delta t^2 C_0 \frac{\partial^2}{\partial y^2}\right)\left(1 - \frac{m_e}{m_i}\frac{\partial^2}{\partial y^2}\right) + \frac{\Delta t^2}{4}\frac{\partial^2}{\partial y^2}\right]\frac{\partial^2}{\partial t^2}\underline{b} + \left(1 - \Delta t^2 C_0 \frac{\partial^2}{\partial y^2}\right)\begin{pmatrix} 0 & 1 \\ -1 & 0 \end{pmatrix}\frac{\partial^2}{\partial y^2}\frac{\partial}{\partial t}\underline{b} - \frac{\partial^2}{\partial y^2}\underline{b} = 0$$

- With $C_0 \geq 1/4$ and additional homogenous bcs, the spatial operator acting on the highest temporal derivative is a positive differential operator.
- Electron inertia contributes to this property but is not essential.
- With Fourier expansion, all solutions of the characteristic equation for ω_k^2 are real and positive when $C_0 \geq 1/4$, i.e. stable propagation without numerical dissipation.

Benchmarking of NIMROD with ELITE

Refresher: Two ballooning unstable equilibria with a zero current outer layer were generated with TOQ to avoid mapping errors that plague benchmarking efforts with direct-solver equilibria.

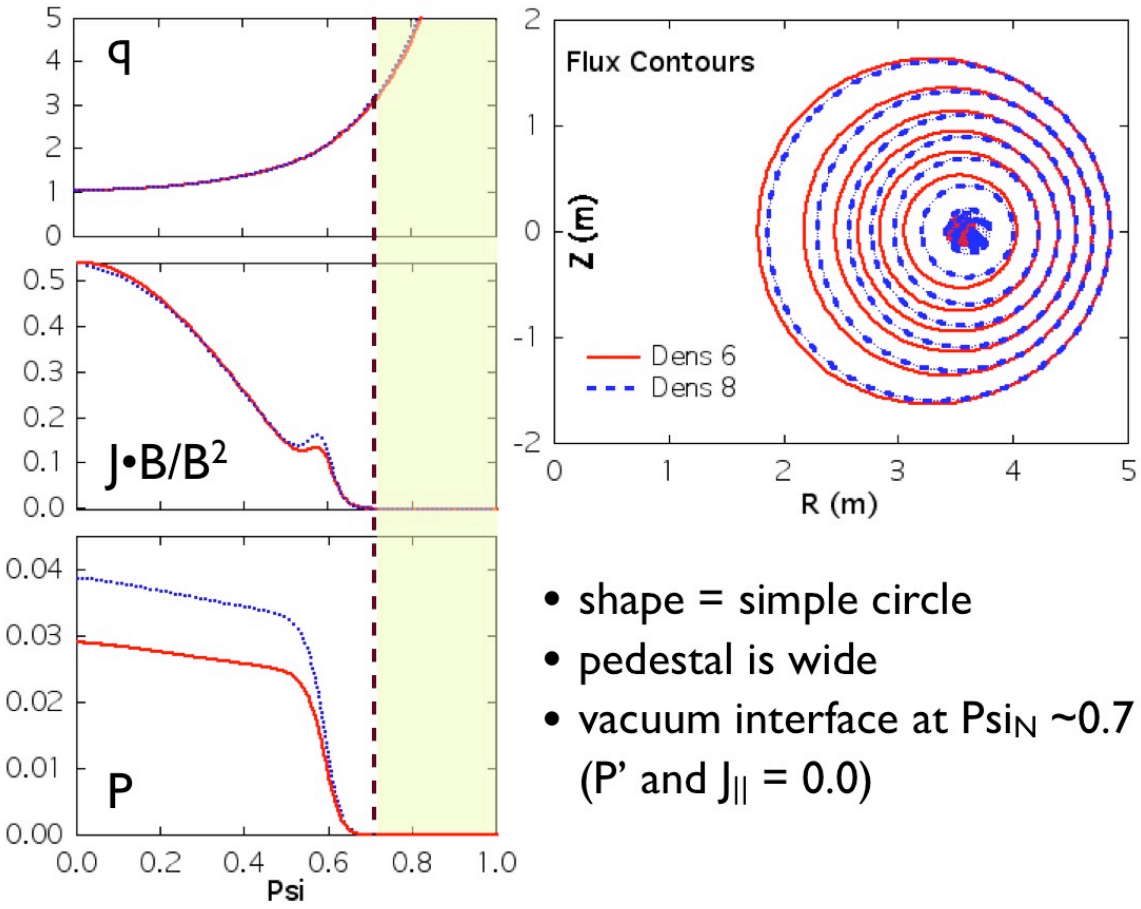

- shape = simple circle
- pedestal is wide
- vacuum interface at Psi_N ~0.7 (P' and $J_{||}$ = 0.0)

• Scans of linear computations determined the S_{in}-value needed for an ideal mode response (>10^8) for representative toroidal harmonics.

• Other scans checked for the maximum S_{out} and the maximum ρ_{halo} needed to obtain a vacuum-like response (<10^3 and <$\rho_{in}/100$ for these cases).

Final results with halo modeling are in quantitative agreement (to the margin between GATO and ELITE).

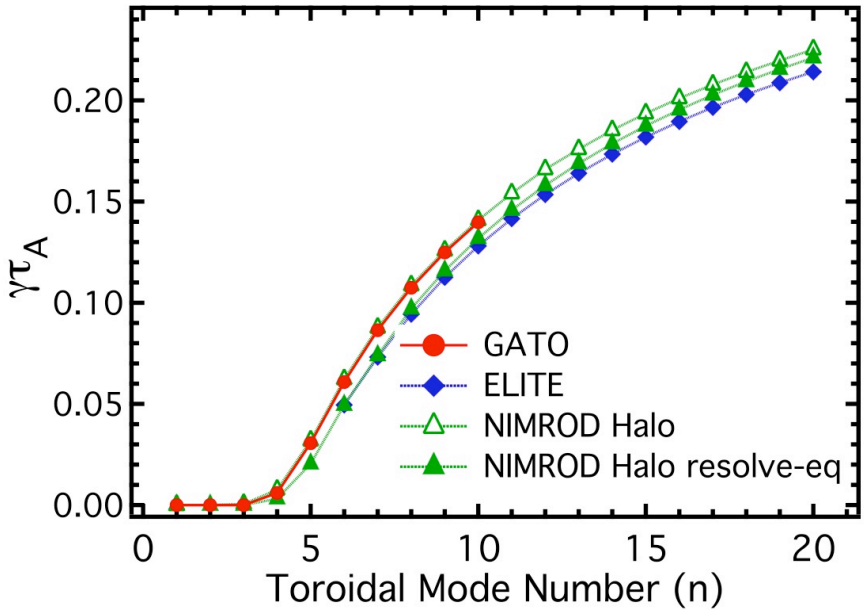

ELITE and GATO results are available for the more unstable, dens8 case.

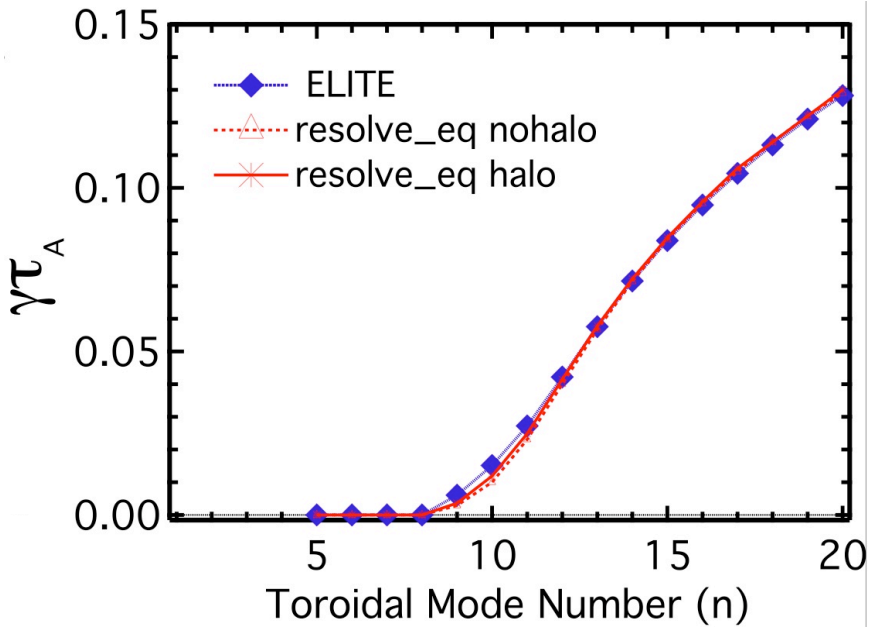

Only ELITE results are available for the less unstable, dens6 case.

- Even with high-resolution TOQ equilibria, re-solving the equilibrium on NIMROD's mesh with NIMEQ vs. interpolation with FLUXGRID makes a quantitative difference in the linear results.
- GATO interpolates to low-order elements; ELITE uses local expansions about each rational surface.
- Halo computations with discontinuous η-profiles work well with element borders aligned with the discontinuity.

Marginal ideal conditions are nontrivial for NIMROD.

• NIMROD's finite element basis functions are continuous, as needed for a conforming representation with a dissipative system.

• The algorithm may converge from the unstable side.

• The mesh for these ballooning-mode computations is concentrated near the pressure gradient.

  • Reliable convergence needs packing over all rational surfaces for a given ballooning mode.

  • Regions left with very coarse resolution can generate growing noise.

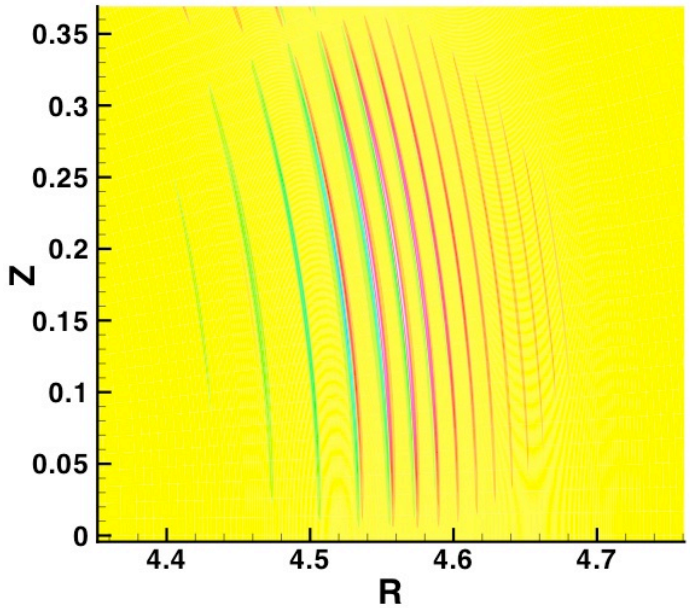

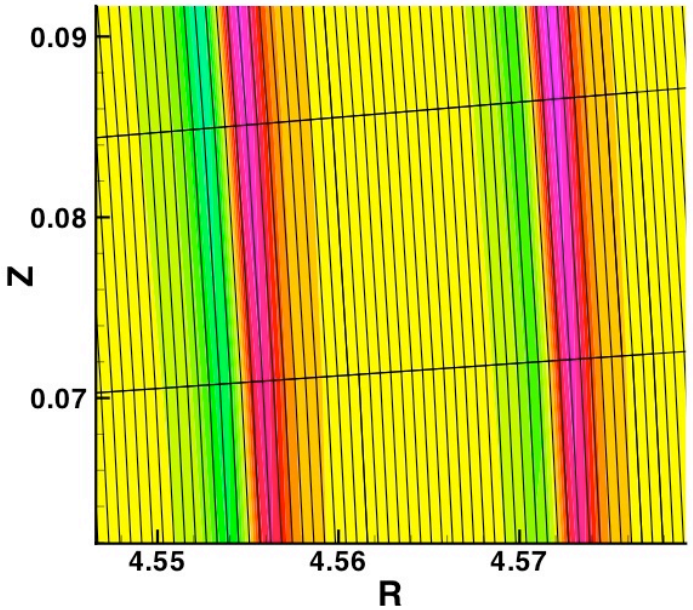

• n=9 dens6 computation needs dissipation with a packed 60×64 mesh and polynomials of degree 7 and is resistive at $S=5.4\times10^{8}$; $\gamma\tau_A=4.8\times10^{-3}$.

Parallel Scaling to 10,000 Cores

Changes made to NIMROD last year lead to the improved scaling.

- Limited Fourier coupling in the preconditioner for the implicit two-fluid B-advance avoids growth of GMRES iteration with increasing toroidal resolution. (figure below)
- Data and loop reordering reduce the number of collective communication calls and increase the data transferred by each call.

Average number of GMRES iterations for the two-fluid magnetic-field advance at a 2-norm tolerance of 10^{-9} for the test computations. Red trace goes from 22 to 342 Fourier components.

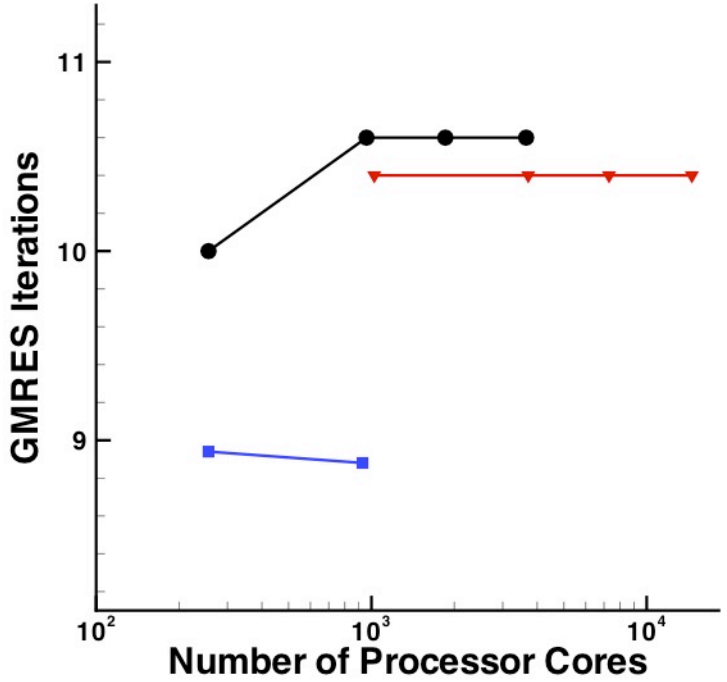

Weak scaling on Franklin shows practical parallel performance to 14,592 processor cores.

- The test is from a 3D cylindrical two-fluid internal kink computation during the nonlinear phase prior to the first crash.
  - $S=10^6$, $\rho_s=0.015a$, $d_i=0.22a$, $d_e=0.005a$
- Tests performed this year do not use the performance monitor IPM.
- Different traces on the figure show 32, 64, and 128 blocks of 16 elements each (polynomials of degree 8).
- The trace with red symbols uses 2 cores per node due to memory limitations with 4 cores per node.
- That trace extends from 22 to 342 Fourier components (8 to 114 'layers').

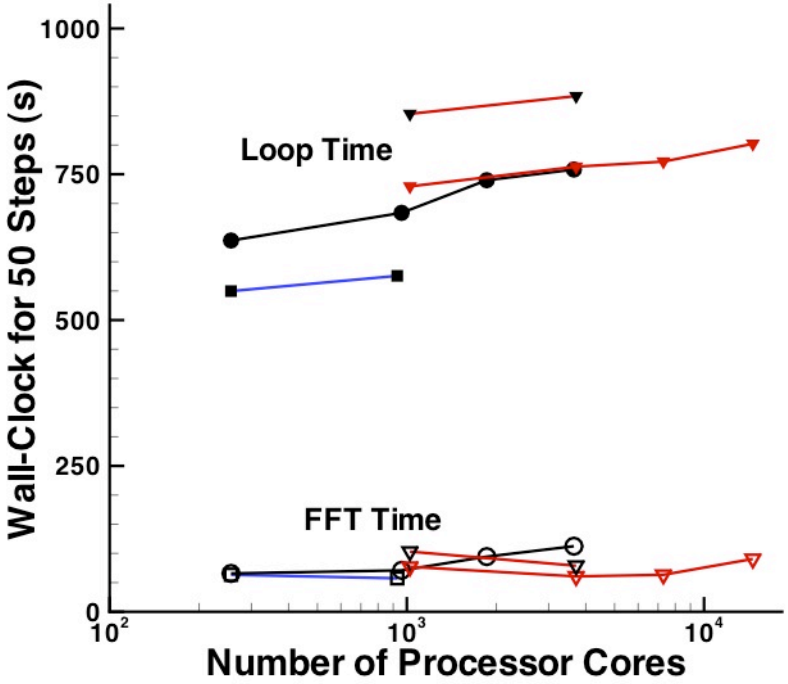

- Jumps between traces reflect operation count and communication with the parallel sparse-direct solver, SuperLU_DIST.
- Tests with Xiaoye Li's new ILU option (serial so far) are encouraging.
- Tech-X is also investigating multi-grid as an alternative.

List of NIMROD-related presentations at APS-DPP 2009

1. CO4.00010 Izzo, Studies of Runaway Electron Confinement in MHD Disruption Simulations
2. CP8.00034 Woodruff Toroidal plasma start-up, refluxing and sustainment by repetitive plasma injection
3. CP8.00035 Macnab Extended MHD simulations of repetitive spheromak injection for non-inductive start-up and sustainment
4. GP8.00043 Ji, Perfecting Braginskii's eletron transport coefficients for high collisionality plasmas
5. GP8.00044 Kim, Hybrid Kinetic-MHD Studies of ICC Devices using Lorentz PIC in Finite Elements
6. GP8.00048 Milroy, Nimrod Simulations of FRC Formation with Rotating Magnetic Field Current Drive
7. GP8.00049 Nelson, Simulation and Visualization Progress of the PSI-Center Interfacing Group
8. GP8.00050 O'Bryan Numerical Simulation of Non-inductive Startup and Flux Compression in the Pegasus Toroidal Experiment
9. GP8.00058 Jenkins, Modeling ECCD/MHD coupling using NIMROD, GENRAY, and the Integrated Plasma Simulator
10. GP8.00061 Sharma, Neoclassical parallel closures for toroidal plasmas
11. GP8.00093 Schlutt, Investigation of equilibrium plasma beta limits in 3D magnetic topologies
12. GP8.00095 Takahashi, Kinetic Effects of Energetic Particles on Nonlinear Resistive MHD Stability
13. GP8.00099 Kruger, Toroidal Mode Coupling in Tokamaks with Anisotropic Viscosity
14. NP8.00113 Burke, Peeling-Ballooning Mode Analysis in Shifted-Circle Tokamak Equilibria
15. NP8.00114 Schnack, Numerical Simulation of Giant Sawteeth in Tokamaks Using the NIMROD Code
16. PI2.00006 Whyte, Runaway Electron Transport and Disruption Mitigation Optimization on Alcator C-Mod
17. PP8.00101 Bird, Numerical Simulations of Current Channel Relaxation For Non-Inductive Startup
18. TP8.00071 King, Numerical Studies of Two-Fluid Tearing and Dynamo in a Cylindrical Pinch
19. TP8.00073 Khalzov, Relaxed states and finite pressure effects in the reversed field pinch
20. TP8.00135 Cheng, Progress in kinetic MHD simulation of magnetic reconnection in Harris sheet equilibrium
21. UP8.00023 Akcay, NIMROD Simulations of HIT-SI Plasmas
22. UP8.00025 Hooper, Refluxing physics for quasi-steady state spheromak sustainment
23. UP8:00026 LoDestro, Simulation of multipulsed edge-current in SSPX
24. UP8.00034 Howell, Extended MHD Simulations of Interchange Modes in Spheromak Equilibria
25. UP8.00082 Held, Continuum solution of the drift kinetic equation in NIMROD
26. UP8.00092 Zhu, Nonlinear Ballooning Instability in the Vicinity of a Separatrix
27. UP8.00100 Brennan, Toroidal flow effects in 3/2 and 2/1 resistive modes nonlinearly driven by a 1/1 internal kink
28. UP8.00101 Montgomery, Resistive Wall Mode Studies in NIMROD
29. UP8.00124 Ebrahimi, Numerical simulations of the Plasma Couette Flow Experiment
30. XI3.00004 Hollmann, Experiments in DIII-D Toward Achieving Rapid Shutdown with Runaway Electron Suppression
31. XP8.00069 Tarditi, Modeling of the Lightning Plasma Channel Stroke to a Spacecraft during Ascent
32. XP8.00070 Tarditi, FRC Formation and Stability in an Accelerated Plasma Flow

Conclusions

- Differential approximation supports the key findings of von Neumann analysis for the implicit leapfrog.
    - Expanding about separate time-levels is useful but requires terms that account for synchronization.
- NIMROD's two-fluid plane-wave responses at large Δt have been verified by initializing with eigenmode information from von Neumann analysis.
- Benchmarking with ELITE on ballooning-unstable equilibria is complete.
    - There is quantitative agreement, but computations near ideal marginality need careful meshing.
- With effective preconditioning, Fourier representation is not an impediment to parallel scaling.